An Ultrawideband Dual-Polarized Phased Array Antenna for Sub-3–GHz 5G Applications With a High Polarization Isolation

De-Ming Sun, *Graduate Student Member, IEEE*, Zhang-Cheng Hao, *Senior Member, IEEE*, Wen-Ye Liu, *Graduate Student Member, IEEE*, and Chen-Yu Ding, *Graduate Student Member, IEEE*

***Abstract*— A dual-polarized ultrawideband (UWB) phased array antenna with a wide scanning range and high isolation polarization characteristics is presented in this article. A tightly coupled dipole with an etched slot is proposed as the element antenna, which has a low active input impedance in a wideband and a wide scanning range. Thus, a simple feed strategy without requiring additional external matching networks and baluns could be adopted for the designed scheme. To obtain a large polarization isolation, a capacitively loaded cross-shaped metallic wall (CSMW) is proposed. It is also helpful to improve the in-band matching by mitigating the bandwidth-limiting loop mode at lower frequencies and removing the undesirable common-mode resonance. As a demonstration, an array is designed with a 4.1:1 bandwidth (0.69–2.88 GHz) and an active VSWR < 3.4 while scanning up to ±45° in the E-, H-, and D-planes. Its polarization isolation is better than 45 dB at the broadside and 35 dB within most of the bandwidth when scanning to ±45° in the E-/H-planes. Its cross-polarization level is more than 51 dB at broadside and 40 dB in scanning up to ±45° in the E- and H-planes. A dual-polarized 8 × 8 array prototype (64 ports per polarization) is manufactured and evaluated. Results from the experiment demonstrate good agreement between the measurement and design. The designed antenna is scalable and has a high polarization isolation, a wide scanning range, an ultrawide bandwidth, and a low cost.**

***Index Terms*— Dual-polarized array, high polarization isolation, phased arrays, ultrawideband (UWB), wide-angle scanning.**

I. Introduction

RECENTLY, the fifth-generation (5G) wireless communication technology has exploded in various wireless applications due to its huge data transmission rate and low latency [1]. Currently, 5G technology uses a variety of frequencies within the sub-6 GHz and above 24 GHz [millimeter wave (mm wave)] range. While the mm wave offers a larger spectrum, it suffers from coverage due to path loss and building penetration [2]. As a result, the sub-6 GHz is preferred for long- and wide-range coverage. With the rise of the 5G MIMO technology, new frequency bands are allocated for 5G applications recently. For example, the 700 MHz, 900 MHz, and the 2.6 GHz frequency bands have been licensed for the commercial 5G application in China. The sub-3–GHz 5G system could be used for large coverage and must be compatible with other wireless systems, such as the 3G, 4G, and GSM systems. As a consequence, a major challenge is to develop multiband wide-angle scanning antennas, so that the existing standard antennas can be integrated with the 5G new radio (NR). Generally, multiple antennas have to be adopted for the sub-3–GHz 5G system, which not only requires a significant cost but also increases the system complexity, size, and weight. Furthermore, the dual-polarized wide-angle scanning array antennas are essential in 5G applications because of their advantages of alleviating multipath fading, enhancing channel capacity, and increased reliability [3], [4], and arrays with high polarization isolation, ultrawide bandwidth, large scanning range, and easy integration are always the challenge for simultaneous transmit and receive (STAR) systems [5]. Hence, it is desired that a single antenna could be used for the full system, which is expected to have an ultrawide bandwidth converging from 700 MHz to 3 GHz, multiple beams with a wide scanning range, dual-polarized capability, and large polarization isolation.

To develop ultrawideband (UWB) phased arrays, various methods have been employed. One of the most widely utilized wideband arrays is the Vivaldi array in UWB systems [6], [7], [8], [9], [10]. However, it requires a large and tapered opening associated with an excess weight and a large volumetric size, especially at lower frequencies. Another attractive wide bandwidth topology is the tightly coupled dipole array (TCDA) based on Wheeler's current sheet theory [11], [12], [13], [14], [15], [16]. In general, the TCDAs can be classified as vertically integrated and fully planar topologies. However, the vertically integrated arrays need to be configured with lossy, bulky, and complex UWB feeding networks, which is always challenging when

Manuscript received 4 November 2022; revised 29 January 2023; accepted 31 January 2023. Date of publication 2 March 2023; date of current version 5 May 2023. This work was supported in part by the National Natural Science Foundation of China under Grant 62131008 and in part by the Fundamental Research Funds for the Central Universities under Grant 2242022k30003. *(Corresponding author: Zhang-Cheng Hao.)*

De-Ming Sun, Wen-Ye Liu, Chen-Yu Ding are with the State Key Laboratory of Millimeter-Waves, Frontiers Science Center for Mobile Information Communication and Security, School of Information Science and Engineering, Southeast University, Nanjing 210096, China (e-mail: demingsun@seu.edu.cn; wyliu@seu.edu.cn; cyding@seu.edu.cn).

Zhang-Cheng Hao is with the State Key Laboratory of Millimeter-Waves, Frontiers Science Center for Mobile Information Communication and Security, School of Information Science and Engineering, Southeast University, Nanjing 210096, China, and also with the Purple Mountain Laboratories, Nanjing 211111, China (e-mail: zchao@seu.edu.cn).

Color versions of one or more figures in this article are available at https://doi.org/10.1109/TAP.2023.3249342.

Digital Object Identifier 10.1109/TAP.2023.3249342

the physical space is limited, especially at lower frequencies. Furthermore, in order to suppress the common mode of the array, a loss (>3 dB) resistive card (R-Card) has to be adopted [15].

Compared with the vertically integrated arrays, the quasi-full planar configurations including the planar UWB modular antenna (PUMA) arrays [17], [18], [19], [20], [21] and connected slot arrays (CSAs) could be manufactured by using the standard printed-circuit-board (PCB) process and have the advantages of a compact size and lightweight [22], [23], [24], [25], [26]. The external matching circuit and shorting posts are usually adopted in the full-planar UWB array design for removing the resonant mode and expanding the operational frequency bandwidth [17], [18], [19], [20], [21], [22], [23], [24], [25], [26], which, however, is hard to implement at very low frequencies.

Recently, we presented a UWB antenna array utilizing the transversely connected folded tightly coupled dipoles (TCF-TCDA) with low-profile and wide-angle scanning characteristics [27]. This consists of an array of TCF-TCDA with a wide-angle impedance matching (WAIM) layer as a superstrate, with a broadside bandwidth of 0.41–3.3 GHz (8:1). The antenna element has a simple feeding structure and can be directly fed by a coaxial cable. Through the introduction of a capacitively loaded metallic wall, the common mode resonance is suppressed. However, the additional thick dielectric superstrate or the WAIM layer significantly increases the profile, complexity, weight, and cost. More importantly, the transversely connected topology of the antenna cannot be applicable to the dual-polarized design.

In this work, an innovative wide-scanning and UWB dual-polarized phased array antenna is presented to address the aforementioned challenges for sub-3–GHz 5G applications. The presented array performs with low cross-polarization and excellent polarization isolation, as well as the merits of lightweight, low complexity, more economical, and convenient manufacturing and assembling.

The arrangement of this article is as follows. The architecture, evolution, and development of the suggested antenna are detailed in Section II. The experimental verification results of an 8 × 8 dual-polarized array prototype are discussed in Section III, and a comparison of the presented design to other dual-polarized UWB arrays is compiled. Finally, conclusions are reached in Section IV.

II. Antenna Element and Design Process

A. Array Element Structure

Fig. 1 depicts the basic block of the presented array antenna, which composes of 2 × 2 tightly coupled dipoles and the detailed configuration of the dual-polarized element. The element antenna consists of a horizontal bowtie structure and a vertical structure, which are connected to each other. Both the vertically (V-Pol) and horizontally (H-Pol) polarized bowtie sections located on the same layer are printed on the bottom layer of Rogers RO4003 dielectric substrate (relative dielectric permittivity $\varepsilon_r = 3.55$, loss tangent tan $\delta = 0.002$, and thickness $t = 0.813$ mm). The vertical structure of the element

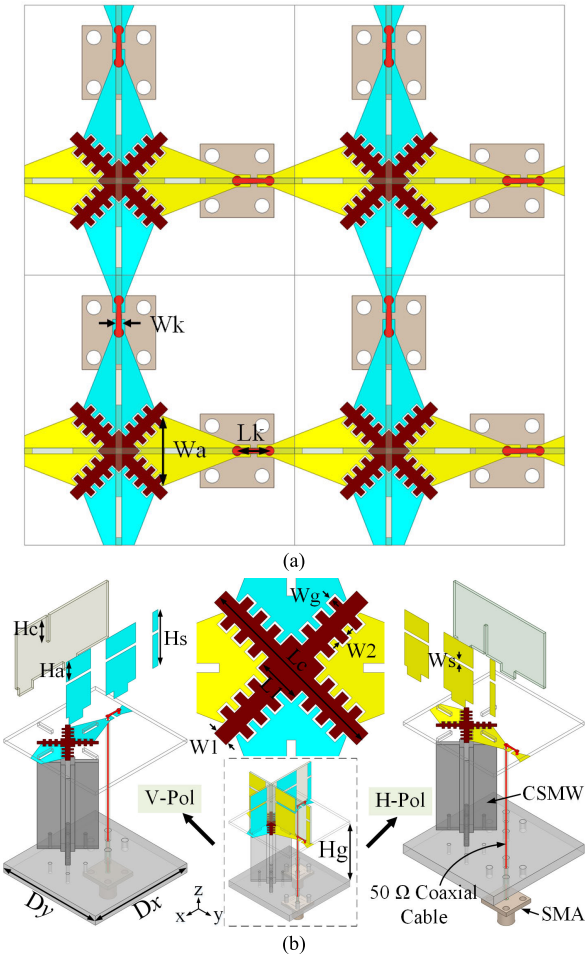

Fig. 1. Architecture of the presented dual-polarized antenna with actual feed configuration. (a) Top view of 2 × 2 unit array. (b) Illustration of its elements.

antenna is printed on the side of the Rogers RO4003 dielectric substrate with a thickness of 0.508 mm. The end of the bowtie sections and the crossed fishbone strip on the same layer form the interdigitated capacitance to enhance the low-frequency limit of the working band. To eliminate the common-mode resonance and avoid the bandwidth restriction produced on lower frequency loop modes, a cross-shaped metallic wall (CSMW) is introduced, whose position is between the antenna and the ground plane, and its upper surface is in contact with the crossed fishbone directly above it. A typical 50 Ω coaxial cable is employed to feed the array unit directly to a short-circuited microstrip line engraved on the upper layer of a horizontal dielectric substrate. Screws are used to assemble the antenna. To improve the impedance-matching performance when scanning at large angles, a slot is etched in the vertical part of the antenna. The size of the element is 46.5 × 46.5 × 64.1 mm, and the final key dimensions are provided in Table I.

B. Bandwidth Improvement

Fig. 2 shows the evolution of the proposed array antenna from the conventional dual-polarized TCDA in [17], [18], [19], [20], and [21]. The typical bowtie dual-polarized TCDA, as Ant.1, is presented with a metallic ground plane. The UWB property is achieved by canceling the inductance introduced

TABLE I
GEOMETRY PARAMETERS (UNIT: mm)

Parameters	Value	Parameters	Value	Parameters	Value
D*x*	46.5	Hc	12.3	Wa	12.1
D*y*	46.5	Hs	25.3	Lc	22.1
Hg	38	L1	5.1	Ws	1.4
W1	1.8	Wc	5	Lk	5.58
W2	1	Wk	1	Ha	8.7

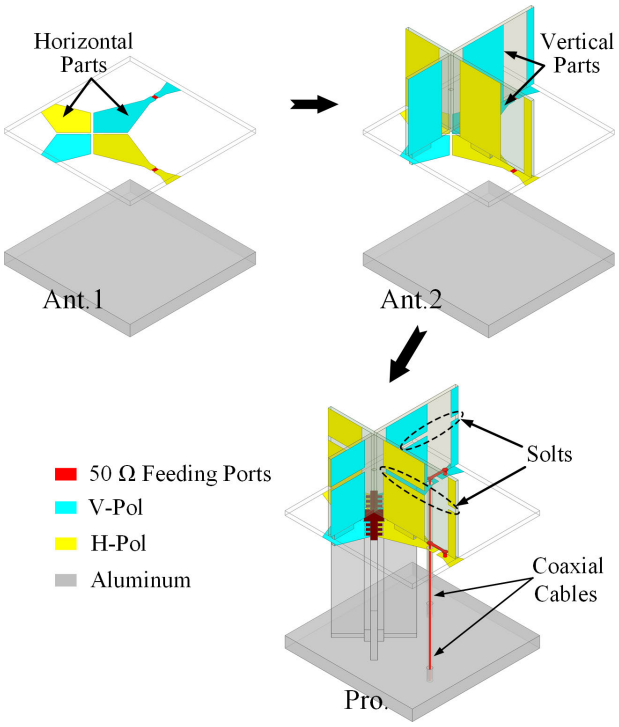

Fig. 2. Evolution concept for the proposed antenna.

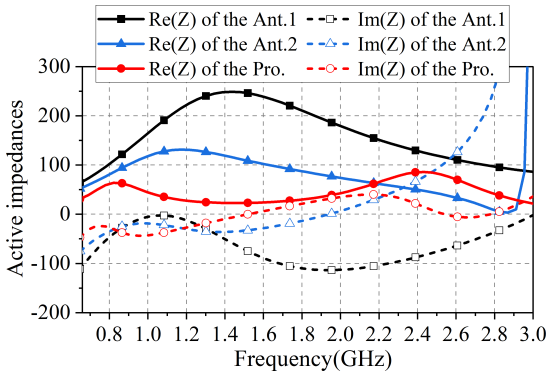

Fig. 3. Active impedances of the Ant. 1, Ant. 2, and Pro.

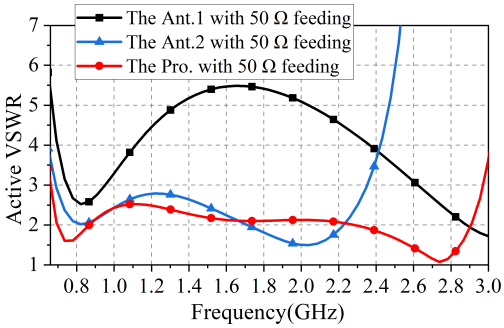

Fig. 4. Active VSWRs of the Ant. 1, Ant. 2, and Pro.

by the ground reflector through the capacitive coupling formed between adjacent dipoles. However, the TCDAs have a very large input impedance in practice [17] that makes it necessary to have an impedance-matching network when fed with a 50 Ω source. In order to directly match the antenna with 50 Ω and avoid the complex feeding network, the vertical part is introduced as another part of the antenna, which is connected with the horizontal part, as shown the Ant. 2. Fig. 3 compares the active input impedances of Ant. 1 and Ant. 2 in an infinite array. Obviously, Ant. 2 has a lower active input impedance than Ant. 1, making it easier to match to 50 Ω without any additional impedance transformation, and the addition of a vertical part makes the wideband impedance matching performance of the traditional TCDA significantly improved, as is depicted in Fig. 4. As can be observed, although the bandwidth of Ant. 2 has been improved, its resistance is still relatively large and the impedance becomes inductive at upper frequencies. Therefore, we further etched slots in the vertical part of Ant. 2 to generate capacitance, which can cancel out the inductive, resulting in significantly improved bandwidth, especially for the upper frequencies band, as shown in Fig. 4.

Note that Ant. 1 and Ant. 2 are fed with 50 Ω ideal lumped ports and the Pro. is fed with the 50 Ω coaxial cables in the infinite array setting. The height between antenna layer and aluminum reflector is kept the same for a fair comparison. In addition, it is worth mentioning that the added vertical part with slots of the antenna benefits to improve the wide angle matching, which will be discussed further in the following.

C. Analysis of the CSMWs

1) Common-Mode Suppression: The common-mode suppression is very important for achieving a wide operating band for the TCDA. An interesting technique using the shorting pins on the arm of the dipole shows the good common-mode suppression capability [13], [17], [18], [19], [24], [25], [26]. For the single-polarization TCDA using vertically integrated dipoles [13], [28], [29], adopting a single shorting pin is enough for suppressing the common mode. However, this type of TCDA requires a complicated feed balun connected with the shorting pins. It increases the feed loss, the antenna size, and the assemble difficulty. On the other hand, for the single-polarization TCDA using horizontally integrated dipoles [17], [18], [19], [25], [26], density shorting pins are required for the common-mode suppression, which is very difficult for the very low-frequency application. In addition, the shorting pins would introduce a resonant loop mode between elements, which limits the lowest cutoff frequency of the antenna. More importantly, for the dual-polarization TCDA with integrated vertical and horizontal dipoles, although the common mode can be suppressed by using the shorting pins, the polarization isolation is poor for applications [18], [30].

As shown in Fig. 5, the common-mode resonant of the proposed array is about 2.38 GHz. To achieve a wideband

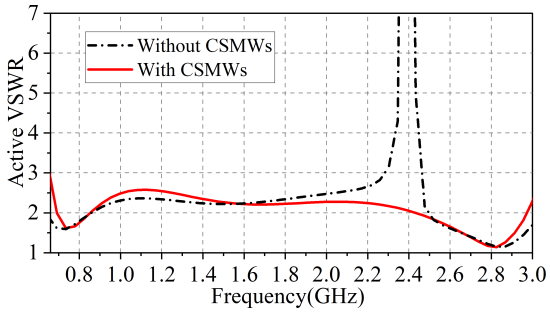

Fig. 5. Simulated VSWRs of a unit cell without and with the CSMWs.

common-mode suppression and improve the polarization isolation, a CSMW shown in Fig. 2 is introduced in the design. In the design of Ant. 1 and Ant. 2, the gap between the ends of the dipoles is used to strengthen the mutual coupling for achieving a wide bandwidth, and the location between the dipoles and the aluminum reflector is 38 mm. When a CSMW is introduced, to compensate the required coupling for obtaining a wide bandwidth, the metallic wall is not attached to arms of the element, which instead keeps a small slit Wg to realize capacitive loading, as illustrated in Fig. 1(b). The ground and dipoles spacing remains as 38 mm, which is the same as the height of the metallic wall Hg. For achieving the assembling quality and machining accuracy, the thickness W1 of the CSMW is designed as 1.8 mm for machining fabrication. In order to obtain enough capacitive coupling between the CSMW and antenna elements for realizing a wide bandwidth performance, the crossed fishbone strip is designed as connected with the CSMW to form the interdigitated capacitance. Thus, without further alignment, the substrate of the antenna can attach precisely, preventing element-to-element offsets and fabrication mistakes. Based on the above considerations, the parameters Wg, Lc, L1, and W2 of the CSMW have been tuned for obtaining a good radiation and impedance matching performance.

Consequently, the problematic resonant is suppressed and the UWB performance of the antenna is achieved, as illustrated in Fig. 5. To explain this more clearly, the surface current magnitude distributions of the horizontal dipoles and the *E*-field along dipoles E-plane are presented in Fig. 6 at 2.38 GHz. While the H-Pol element is matched, the V-Pol element is excited. As depicted in Fig. 6(a), without CSMWs, the V-Pol dipoles have no differential current at the common-mode resonant and are in a nonradiation mode. However, when the CSMWs are introduced, the common mode of the array is eliminated and the current of the dipoles is restored to the differential, resulting in the radiation mode, as shown in Fig. 6(b). In addition, the introduced metallic walls can act as a support for the antenna, which avoids the use of foam, increases the mechanical strength and avoids bulky of the antenna, and also reduces the complexity of installation.

2) Polarization Isolation Enhancing: Achieving a large polarization isolation within UWB is always the challenge for developing the dual-polarization array antenna. The mutual coupling between the cross-dipole elements mainly includes three components: the coupling between the feeding networks, the coupling between the antenna elements, and the

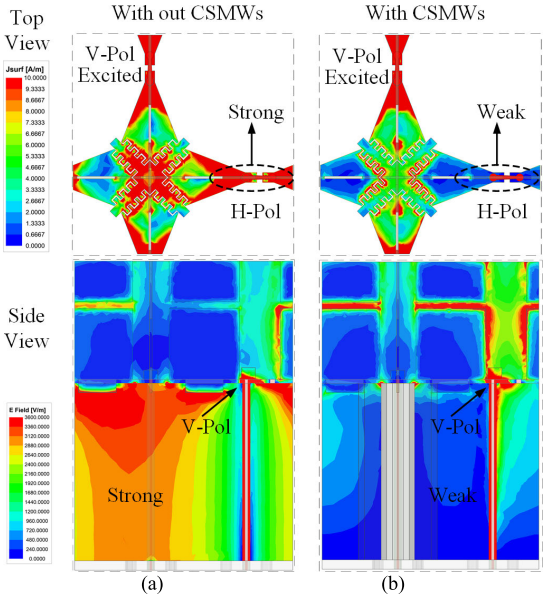

Fig. 6. Comparison of magnitude distribution of surface current and *E*-field along E-plane of V-Pol component at 2.38 GHz. (a) Pro. without the CSMWs. (b) Pro. with the CSMWs.

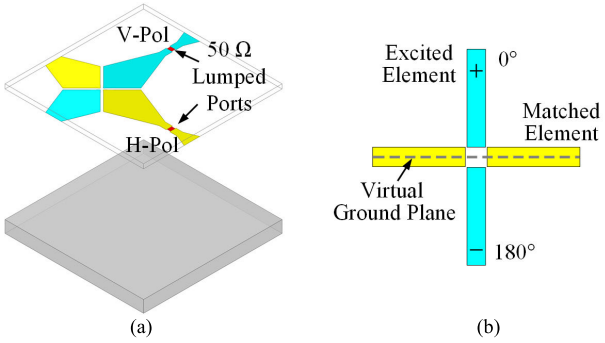

Fig. 7. Configuration of the orthogonal dipole elements with ideal feeding ports. (a) Ant. 1. (b) Feeding arrangements.

coupling between the feeding network and the antenna elements. An integrated Marchand balun with multiple shorting vias is helpful to reduce those coupling [19], but it needs multiple dielectric layers and is not good for low-frequency applications. In this work, we used the CSMWs for achieving a large polarization isolation. It could be explained by the current distribution of the dual-polarized tightly coupled dipole element. When the element is differentially fed illustrated in Fig. 7, the distribution of the electric field is symmetric and the element is in a balanced radiation mode, as shown in Fig. 8. In this case, the current field distribution of the unexcited polarized dipole element is pretty weak. That indicates there is almost no coupling between the two orthogonal dipoles. In this case, the isolation between them is 55 dB at 2.38 GHz, as shown in Fig. 9.

However, when the antenna element is excited by the coaxial cable for practical applications, its balance and symmetry are severely disturbed. In this instance, as shown in Fig. 9, the isolation between the orthogonal dipole elements is only 4 dB at 2.38 GHz. To reduce the influence of the feed network, the CSMWs between the orthogonal dipoles can

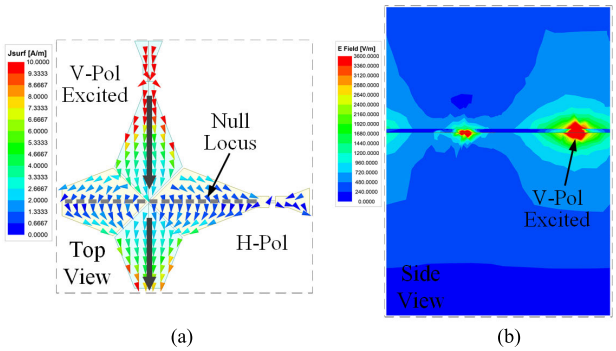

Fig. 8. E-field distribution and surface current of Ant. 1 at 2.38 GHz. (a) Surface current. (b) E-field.

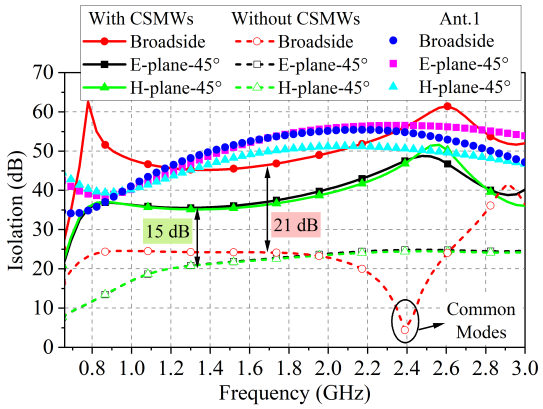

Fig. 9. Comparison of the simulated polarization isolation without and with the CSMWs.

be adopted for shielding the feeding coaxial cables, which is helpful to realize a differential current distribution for the excited dipole element, as shown in Fig. 6(b). This assists in reducing the coupling between the orthogonal dipoles. Fig. 9 shows that the isolation between dual-polarized elements in the desired frequency band reaches 45 dB at the broadside as well as 35 dB while scans to ±45° when the CSMWs are adopted. Compared to the case without CSMWs, the isolation is improved by 20 and 15 dB, respectively.

D. Scanning Range Improvement

Generally, a thick dielectric superstrate has to be placed above the TCDA array antenna for obtaining a wide bandwidth and wide scanning range [17], [20], [21], [22], [23], [24], [25]. However, for low-frequency applications, a very thick superstrate is required that makes the UWB array antenna bulky, heavy, and expensive. To overcome this shortcoming, we etched slots on the vertical part of the element antenna. As seen in Fig. 10, when without the etched slot, the realized bandwidth is only 3.4:1 (0.69–2.4 GHz) when scanning to 45° in all planes with the active VSWR < 3. On the contrary, the operating bandwidth can be extended to 4:1. Although the VSWR level is a little bit greater than that of the case without a slot, it is still within the acceptable range. Obviously, by using the etched slots, the proposed antenna array becomes lighter, more compact, and less costly than using the thick superstrate.

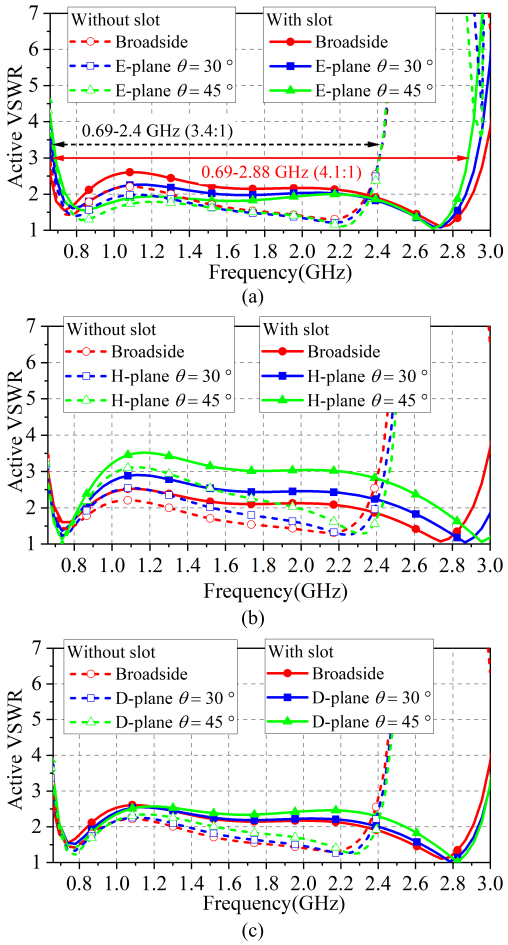

Fig. 10. Simulated active VSWRs for scanning in all planes of an infinite periodic element without and with the slot. (a) In E-plane. (b) In H-plane. (c) In D-plane.

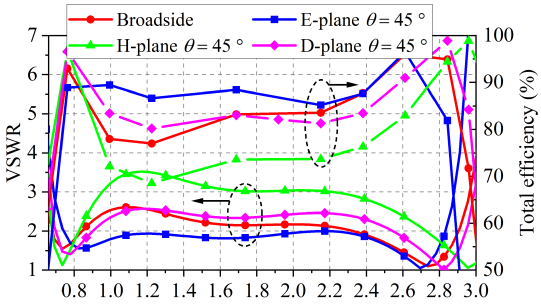

Fig. 11. Simulated active VSWRs and radiation efficiency for scanning in all planes of an infinite periodic element.

E. Simulated Results for the Periodic Element

The capability of the suggested antenna is demonstrated using an infinite array. Fig. 11 shows the computed VSWRs for all scanning planes. The results indicate that the designed antenna could perform more than a bandwidth of 4.1:1 (0.69–2.88 GHz) with active VSWR < 3.4 at scan to ±45° in all planes. In the infinite arrangement, the total radiation efficiency at various scanning angles exceeds 68% across the entire band. Fig. 12 shows the simulated co- and cross-polarization of the presented antenna in all planes. The Ludwig's third definition is implemented to calculate the cross-polarization [31]. In the principal planes, the antenna

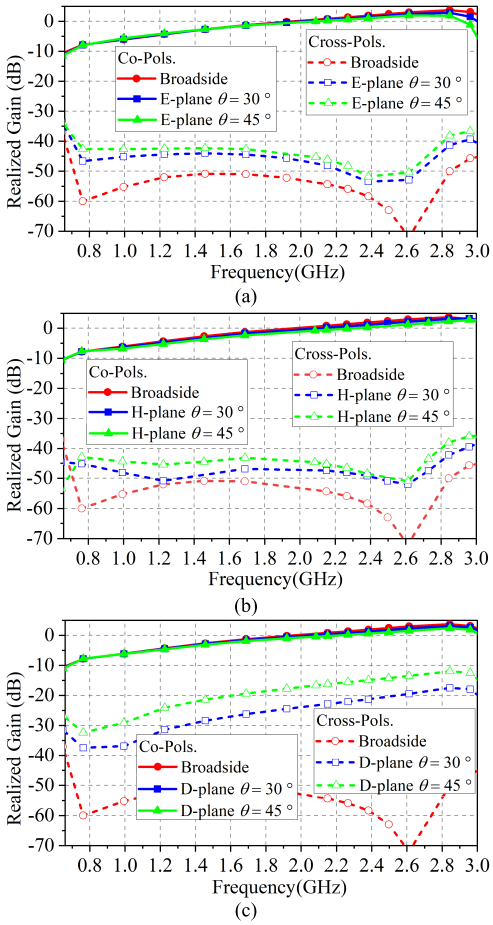

Fig. 12. Simulated co-pol and cross-pol for scanning in all planes of an infinite array. (a) In E-plane. (b) In H-plane. (c) In D-plane.

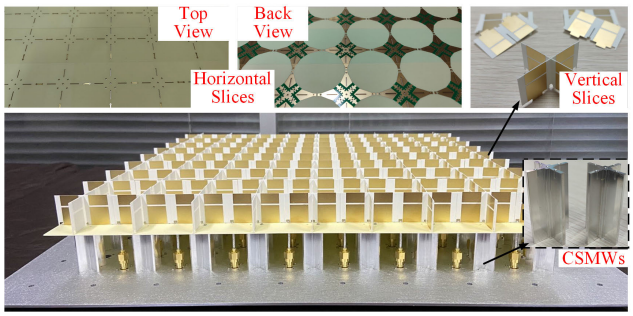

Fig. 13. Photograph of a fully assembled dual-polarized array prototype.

exhibits a very superior cross-polarization when scanning from the broadside to 45°, which is below −40 dB at most of the desired frequencies. This is attributed to the shielding effect of the introduced CSMWs. The cross-polarization in D-plane is higher than in principal planes, especially at large scanning angles [32], i.e., its maximum value is −12 dB at 45°.

III. Validation and Measurement

A. Manufactured Prototype Array

As illustrated in Fig. 13, an 8 × 8 array antenna was manufactured and evaluated. The aluminum ground plane has a thickness of 2 mm, and the overall array component is 497.5 × 497.5 mm; 128 coaxial cables are used to excite all elements; 50 Ω SMA connectors beneath an aluminum plate are connected with SMA-KFK adapters. The CSMWs are fastened to the aluminum plane with screws.

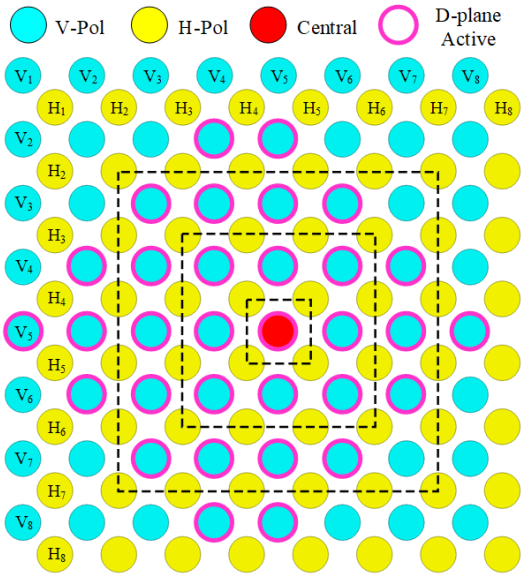

Fig. 14. Schematic of the measurement.

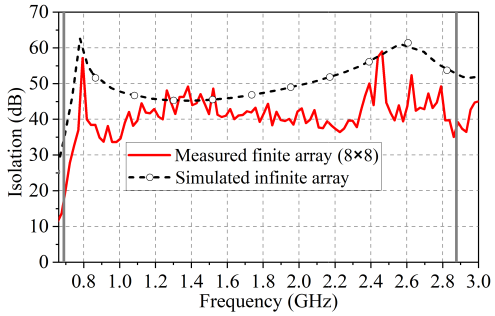

Fig. 15. Measured and simulated polarization isolation at broadside.

B. Polarization Isolation Performance

The isolation between the two polarizations of the TCDAs should take into account mutual coupling from its closest different polarization antennas [33], which can be calculated according to the transfer function (1) representing the coupling from the two different polarized ports, as shown in the following:

$$\mathrm{H}_{pq}(\theta,\phi)=\sum_{m=1}^{M}\sum_{n=1}^{N}S_{mn,pq}e^{-j([m-p]D_x u+[n-q]D_y v)}. \quad (1)$$

In the above, note that the $S_{mn,pq}$ between the components mn and pq with different polarizations is measured. (θ,ϕ) indicates scan angle. The array's E- and H-planes element numbers are M and N, respectively, while the unit lattice size is denoted by D_x and D_y. The coordinates for u–v are given by $v = k_0 \sin\theta_0 \sin\varphi_0$ and $u = k_0 \sin\theta_0 \cos\varphi_0$.

In this case, the coupling between component (V_5, V_5) and its surrounding H-Pol elements on the black dashed lines are measured, as shown in Fig. 14. The H-Pol elements closest to the central elements contribute the majority of the coupling. Therefore, the coupling of elements located in the outermost sphere of the H-Pol can be negligible. Infinite array simulations at broadside are shown in Fig. 15 alongside the

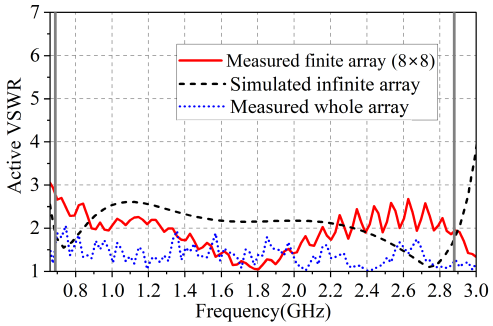

Fig. 16. Design and experiment broadside active VSWRs for center unit (V_5, V_5).

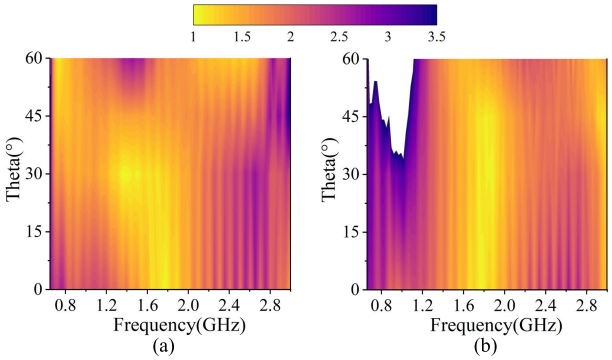

Fig. 17. Experiment active VSWRs of a unit (V_5, V_5) in principal planes. (a) In E-plane. (b) In H-plane.

measured polarization isolation. The measured polarization isolation is below 34 dB across most of the bands. The slightly degradation of the measured isolation level is mostly due to the amplitude and phase errors caused by the imperfect identical coaxial cables in practice [19], [33], as well as the inevitable errors caused by the machining and assembly of the CSMWs.

C. Impedance of a Central Unit

The design results, measurement results and measurement setup for the central unit are shown in Figs. 16–18. All other ports of the same polarization are matched when measuring the S-parameter mutual coupling between specified and central units. Then, the following formula (2) can be used to determine the active reflection coefficient of an element (p, q)

$$\Gamma_{pq}(\theta,\phi)=\sum_{m=1}^{M}\sum_{n=1}^{N}S_{mn,pq}e^{-j([m-p]D_x u+[n-q]D_y v)} \quad (2)$$

where the parameter $S_{mn,pq}$ represents the measured values between components pq and mn with the same polarization.

Fig. 16 shows the infinite array simulations at the broadside alongside the measured active VSWRs of the component (V_5, V_5). It can be seen that the measured VSWRs at some frequencies deteriorate compared to the simulation, which is consistent with the prediction that measurements of small finite arrays nearly invariably reveal greater return loss level than infinite cases [34], [35]. Nevertheless, it is below 3.0 across the full operating band.

The VSWRs of the full array are below 2 across the desired frequency band. Fig. 17 illustrates the results of the central element measured active VSWRs versus frequencies

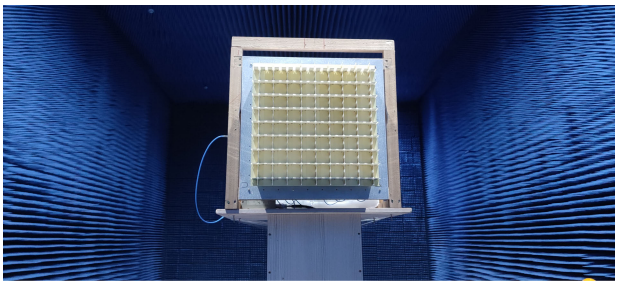

Fig. 18. Measurement scenario for the prototype.

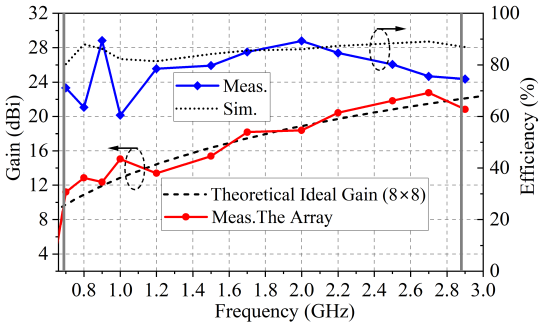

Fig. 19. Measured broadside gain and aperture efficiency of the whole array compared with the simulation results.

and scanning angles in principal planes. When scanning at some frequencies, the measured active VSWR values degrade slightly, showing a larger VSWR level. The main reason for these discrepancies is array-guided surface waves (AGSWs), which usually occur in a finite array [36]. By expanding the scale of the array [34], or adding more parasitic "dummy" elements around the array [37], and so on, the edge effect of finite arrays could be alleviated. In addition, manufacturing tolerances, assembly errors, and numerous repeated measurements may lead to disparities between the results of simulation and measurement.

D. Radiation Characteristics

1) Peak Gains and Aperture Efficiency: The broadside peak gains are evaluated as

$$RealizedGain=\frac{4\pi NA\left(1-|\Gamma|^2\right)}{\lambda^2}. \quad (3)$$

Fig. 19 compares the measured realized gains versus frequencies of the array at the broadside to the theoretical gains in order to examine the radiation ability of the entire array. As a whole, the measured result agrees well with the theoretical value in the operating band. According to [28] and [38], it can be calculated that the measured aperture efficiency of this antenna array is >60% over the entire frequency band. The oscillations up and down in the measured results are ascribed to the limited array size and the backing reflector [18], [20].

2) Embedded Element Pattern: Figs. 20–22 show the measured (solid line) and simulated (dashed line) embedded element patterns of all planes for central unit (V_5, V_5) at 0.8, 1.4, 2, and 2.6 GHz, respectively. By exciting a central element and

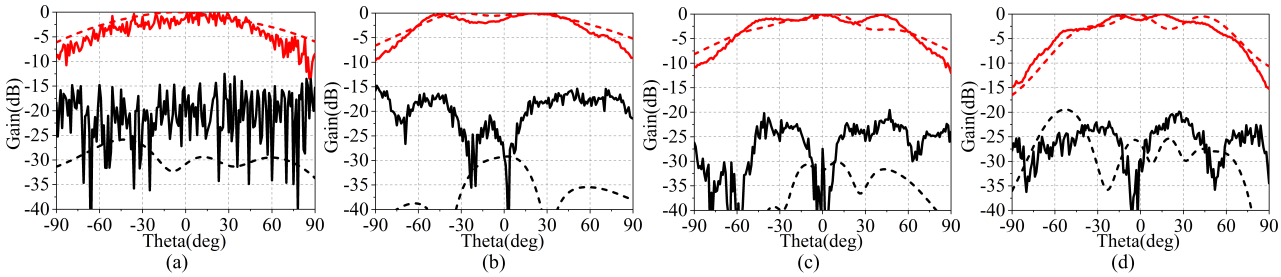

Fig. 20. Experiment and design central component (9, 9) patterns in E-plane. (a) 0.8, (b) 1.4, (c) 2, and (d) 2.6 GHz.

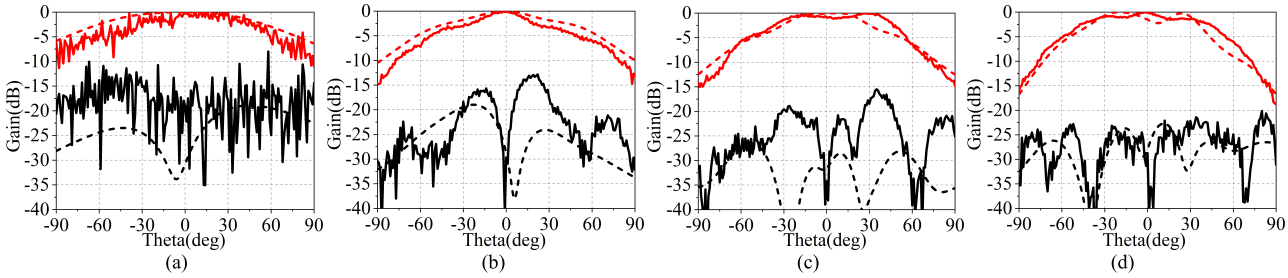

Fig. 21. Experiment and design central component (9, 9) patterns in H-plane. (a) 0.8, (b) 1.4, (c) 2, and (d) 2.6 GHz.

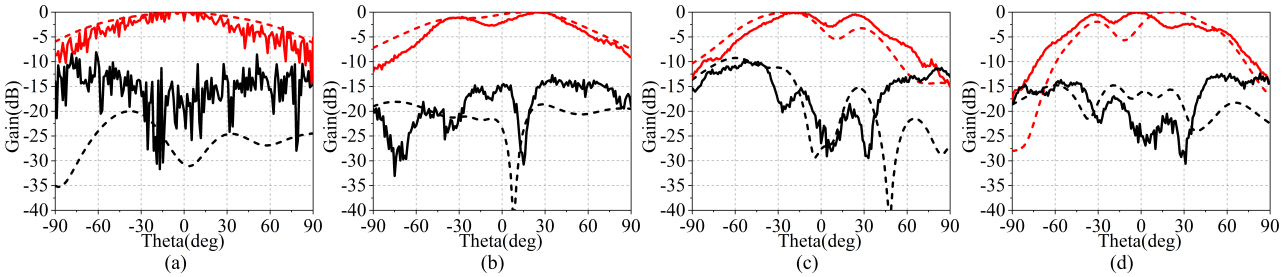

Fig. 22. Experiment and design central component (9, 9) patterns in D-plane. (a) 0.8, (b) 1.4, (c) 2, and (d) 2.6 GHz.

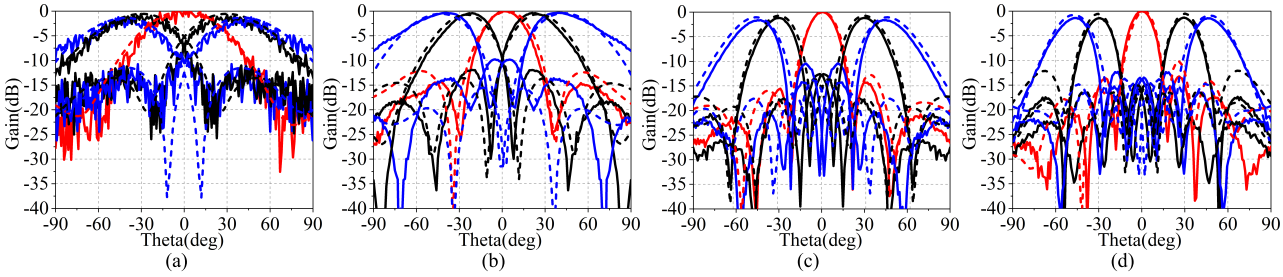

Fig. 23. Experiment and design scanning patterns of the designed 8 × 8 array in E-plane. (a) 0.8, (b) 1.4, (c) and (e) 2, and (d) 2.6 GHz.

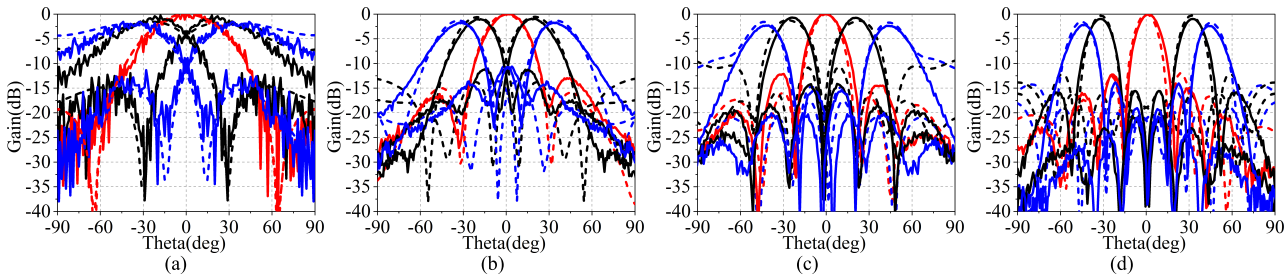

Fig. 24. Experiment and design scanning patterns of the designed 8 × 8 array in H-plane. (a) 0.8, (b) 1.4, (c) 2, and (d) 2.6 GHz.

terminating all other elements in loads, the embedded element patterns can be produced. The results show that the measured co-polarization results and the simulated results match well. The measured cross-polarization is a little bit worse than the simulated. This is mainly due to the difficulty of achieving absolute alignment in the measurement process, whereby slight inaccuracies can result in significant variances in the decibel scale. Also, note that the use of a low-gain horn source at low

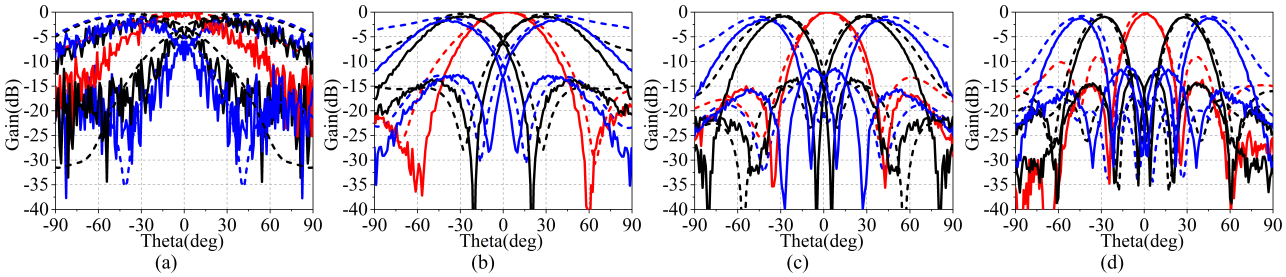

Fig. 25. Experiment and design scanning patterns of the diagonal designed 4 × 8 subarray in D-plane. (a) 0.8, (b) 1.4, (c) 2, and (d) 2.6 GHz.

TABLE II
COMPARISON OF THIS WORK WITH RELATED DUAL-POLARIZATION UWB ARRAYS

Ref.	Impedance Bandwidth	Type of element	Antenna Size	Isolation (broadside)	Cross-Polarization for infinite array (broadside)	Scan Range	*Active VSWR	Common-Mode Mitigation	Feeding Mechanism	#Superstrate Layer	Supporting Layer
[14][2012]	21:1 (0.28-5.91 GHz)	TCDA	4×4	> 27 dB	< -30 dB	N.A.	N.A.	Resistive FSS	Twin Coaxial lines	DS	Yes
[16][2016]	13.5:1 (0.29-3.9 GHz)	TCDA	8×8	> 40 dB	< -40 dB	±45° in all planes	3.1	R-Card	Marchand Balun	DS	Yes
[17][2012]	5:1 (1.06-5.3 GHz)	PUMA	N.A.	> 20 dB	< -20 dB	±45° in all planes	2.9	Shorting Posts	Probe	DS	Yes
[18][2012]	3:1 (7-21 GHz)	PUMA	16×16	> 20 dB	< -25 dB	±45° in all planes	2.9	Plated Vias	Probe	DS	Yes
[19] [2021]	4.5:1 (4-18 GHz)	TCDA	12×12	> 48 dB	< -54 dB	±60° in E-/D-planes ±45° in H-plane	3.4	Shorted Vias	Integrated Balun	MS	Yes
[20] [2018]	6:1 (3.53-21.2 GHz)	PUMA	16×16	> 15 dB	< -30 dB	±60° in all planes	3.8	Capacitively-Loaded vias	Probe	DS	Yes
[23] [2018]	2.5:1 (6-15 GHz)	CSA	16×16	N.A.	< -13 dB	±80° in E-planes ±60° in H-plane	3.0	Plated Vias	Integrated Coax	ADLs	Yes
[30] [2019]	9:1 (2-8 GHz)	TCDA	11×11	> 20 dB	< -40 dB	±60° in all planes	6.0	Shorting Posts	Integrated Balun	FSS	No
[40] [2022]	3.4:1 (0.18-0.62 GHz)	TCDA	12×12	> 35 dB	< -30 dB	±45° in E-/H-planes	3.0	Ferrite Core	Coaxial Cable	No	Yes
This work	**4.1:1 (0.69-2.88 GHz)**	**TCDA**	**8×8**	**> 45 dB**	**< -51 dB**	**±45° in all planes**	**3.4**	**Capacitive Metal walls**	**Coaxial Cable**	**No**	**No**

N.A. refers to not available.
* The active VSWR is the maximum value of the simulation when scanning in an infinite array.
# DS stands for the dielectric superstrate, MS stands for the meta-surface, and ADLs stand for the artificial dielectric layers.

frequencies results in relatively high cross-polarization levels and noisy gains [25], [27], but if a high-gain source above 1 GHz is adopted, the impacts are mitigated. Nevertheless, the measured cross-polarization levels still have a relatively low level for all cases.

3) Patterns of a Finite Array: The scanning performance of the proposed fabricated 8 × 8 prototype array is obtained by applying corresponding phase differences between antenna elements. Figs. 23–25 present the designed (dashed line) and measured (solid line) patterns normalized to peak broadside gain when scanning to broadside, ±30°, and ±45° in all planes. The scanning performance of the D-plane is examined by the excitation of some elements [13], as marked in Fig. 14. Apparently, the measured response of the scanning patterns appears to agree closely with the simulations. Due to bandwidth limitation of the standard antenna in the assessment system, the scanning patterns are measured by using a low-gain standard Yagi-Uda antenna with a frequency below 1 GHz and a high-gain standard horn antenna with a frequency above 1 GHz, respectively. A distance of around 20 m in the microwave chamber is used for the far-field radiation pattern measurement. It is worth mentioning that a low dynamic range of the measurement system is resulted at low frequency by the low-gain Yagi-Uda standard antenna and the undertesting low-gain array element, whose electrical size is just one tenth of the wavelength corresponding to the lowest frequency. That leads ripples in the measured radiation patterns below 1 GHz [27]. When a typical horn with high gain is used, these ripples can be removed above 1 GHz with a relatively large dynamic range of the measurement system. In addition, when the scanning angle becomes wider, the beam pointing error increases, which is due to the beam spreading caused by the small array size. Therefore, the beam pointing accuracy can be improved by increasing the array size [39].

Table II provides a detailed comparison with related dual-polarized phased arrays. All these compared array antennas show good radiation performance. The antennas in [14] and [16] have excellent bandwidth performance, but the use of resistive FSS or R-card adversely affects the antenna radiation efficiency, and their feeding mechanism and assemble process are complicated. The planar UWB antenna array in [17], [18], [19], [20], and [23] has a low profile with stacked multilayer dielectrics, which, however, is not easily scalable for very low-frequency applications. Additionally, it requires external wideband impedance matching circuits or baluns. Although the antenna in [30] has a wide bandwidth and a low cross-polarization at the broadside, its polarization isolation for only 20 dB has a complex feeding network. The antenna in [40] can be directly fed by coaxial cables, but its added ferrite core degrades the antenna gains. Also, compared to the previous partial designs, this design is not bulky as it does not require dielectric covering and supporting layers. In general, the designed array demonstrates a few merits, in aspects of an ultrawide bandwidth, a large polarization isolation, a low cross-polarization level, a simple feed strategy, a low cost, and a low complexity. It is promising for very low-frequency applications.

IV. Conclusion

This work reports a UWB dual-polarized phased array antenna with good cross-polarization and polarization isolation performance. It can be used for lower frequencies applications, e.g., UHF range. The proposed antenna achieves moderate active input impedance over a wide bandwidth, which benefits from the vertical components with slots connected to the horizontal components. Therefore, the proposed antenna does not require complicated impedance transformers and could be fed by a 50 Ω coaxial cable. CSMWs are introduced to eliminate the common-mode resonance occurring in array, broaden the operational bandwidth, and achieve a reduced cross-polarization and excellent polarization isolation. It can decrease the cost and bulk of the antenna, as well as the complexity of the design. For verifications, an 8×8 dual-polarized array prototype is developed, manufactured, and evaluated. Measurement results agree well with the design results. The proposed array can scan to $\pm 45^\circ$ in all planes across 0.69–2.88 GHz (4.1:1) with active VSWR < 3.4. The polarization isolation $> \{45, 32\}$ dB for $\theta = \{\text{broadside}, 45^\circ\}$ scans accordingly. The cross-polarization remained at -40 dB out to $\pm 45^\circ$ scans in the principal planes. The proposed antenna shows that its superior performance not only has a reduced cross-polarization and as well as a large polarization isolation for the STAR systems but also exhibits UWB and wide scanning angles. It has the merits of low cost, lightweight, and simple structure. It can be a potential solution for the sub-3–GHz 5G NR applications.

References

[1] A. Ghosh, A. Maeder, M. Baker, and D. Chandramouli, "5G evolution: A view on 5G cellular technology beyond 3GPP release 15," *IEEE Access*, vol. 7, pp. 127639–127651, 2019.

[2] T. S. Rappaport et al., "Millimeter wave mobile communications for 5G cellular: It will work!" *IEEE Access*, vol. 1, pp. 335–349, 2013.

[3] G. C. Tavik et al., "The advanced multifunction RF concept," *IEEE Trans. Microw. Theory Techn.*, vol. 53, no. 3, pp. 1009–1020, Mar. 2005.

[4] J.-B. Yan, S. Gogineni, B. Camps-Raga, and J. Brozena, "A dual-polarized 2–18-GHz Vivaldi array for airborne radar measurements of snow," *IEEE Trans. Antennas Propag.*, vol. 64, no. 2, pp. 781–785, Feb. 2016.

[5] A. Sabharwal, P. Schniter, D. Guo, D. W. Bliss, S. Rangarajan, and R. Wichman, "In-band full-duplex wireless: Challenges and opportunities," *IEEE J. Sel. Areas Commun.*, vol. 32, no. 9, pp. 1637–1652, Sep. 2014.

[6] N. Schuneman, J. Irion, and R. Hodges, "Decade bandwidth tapered notch antenna array element," in *Proc. Antenna Appl. Symp.*, Monticello, IL, USA, vol. 2, Sep. 2001, pp. 280–287.

[7] D. H. Schaubert, S. Kasturi, A. O. Boryssenko, and W. M. Elsallal, "Vivaldi antenna arrays for wide bandwidth and electronic scanning," in *Proc. 2nd Eur. Conf. Antennas Propag. (EuCAP)*, 2007, pp. 1–6.

[8] A. Ellgardt and A. Wikstrom, "A single polarized triangular grid tapered-slot array antenna," *IEEE Trans. Antennas Propag.*, vol. 57, no. 9, pp. 2599–2607, Sep. 2009.

[9] J. T. Logan, R. W. Kindt, and M. N. Vouvakis, "A 1.2–12 GHz sliced notch antenna array," *IEEE Trans. Antennas Propag.*, vol. 66, no. 4, pp. 1818–1826, Apr. 2018.

[10] J. T. Logan, R. W. Kindt, and M. N. Vouvakis, "Low cross-polarization Vivaldi arrays," *IEEE Trans. Antennas Propag.*, vol. 66, no. 4, pp. 1827–1837, Feb. 2018.

[11] H. Wheeler, "Simple relations derived fom a phased-array antenna made of an infinite current sheet," *IEEE Trans. Antennas Propag.*, vol. AP-13, no. 4, pp. 506–514, Jul. 1965.

[12] J. P. Doane, K. Sertel, and J. L. Volakis, "A wideband, wide scanning tightly coupled dipole array with integrated balun (TCDA-IB)," *IEEE Trans. Antennas Propag.*, vol. 61, no. 9, pp. 4538–4548, Sep. 2013.

[13] E. Yetisir, N. Ghalichechian, and J. L. Volakis, "Ultrawideband array with 70° scanning using FSS superstrate," *IEEE Trans. Antennas Propag.*, vol. 64, no. 10, pp. 4256–4265, Oct. 2016.

[14] W. F. Moulder, K. Sertel, and J. L. Volakis, "Superstrate-enhanced ultrawideband tightly coupled array with resistive FSS," *IEEE Trans. Antennas Propag.*, vol. 60, no. 9, pp. 4166–4172, Sep. 2012.

[15] A. D. Johnson, J. Zhong, S. B. Venkatakrishnan, E. A. Alwan, and J. L. Volakis, "Phased array with low-angle scanning and 46:1 bandwidth," *IEEE Trans. Antennas Propag.*, vol. 68, no. 12, pp. 7833–7841, Dec. 2020.

[16] D. K. Papantonis and J. L. Volakis, "Dual-polarized tightly coupled array with substrate loading," *IEEE Antennas Wireless Propag. Lett.*, vol. 15, pp. 325–328, 2015.

[17] S. S. Holland and M. N. Vouvakis, "The planar ultrawideband modular antenna (PUMA) array," *IEEE Trans. Antennas Propag.*, vol. 60, no. 1, pp. 130–140, Jan. 2012.

[18] S. S. Holland, D. H. Schaubert, and M. N. Vouvakis, "A 7–21 GHz dual-polarized planar ultrawideband modular antenna (PUMA) array," *IEEE Trans. Antennas Propag.*, vol. 60, no. 10, pp. 4589–4600, Oct. 2012.

[19] J. X. Sun, Y. J. Cheng, and Y. Fan, "Planar ultra-wideband and wide-scanning dual-polarized phased array with integrated coupled-Marchand balun for high polarization isolation and low cross-polarization," *IEEE Trans. Antennas Propag.*, vol. 69, no. 11, pp. 7134–7144, Nov. 2021.

[20] J. T. Logan, R. W. Kindt, M. Y. Lee, and M. N. Vouvakis, "A new class of planar ultrawideband modular antenna arrays with improved bandwidth," *IEEE Trans. Antennas Propag.*, vol. 66, no. 2, pp. 692–701, Feb. 2018.

[21] R. W. Kindt and B. T. Binder, "Dual-polarized planar-printed ultrawideband antenna array on a triangular grid," *IEEE Trans. Antennas Propag.*, vol. 68, no. 8, pp. 6136–6144, Aug. 2020.

[22] W. H. Syed, D. Cavallo, H. T. Shivamurthy, and A. Neto, "Wideband, wide-scan planar array of connected slots loaded with artificial dielectric superstrates," *IEEE Trans. Antennas Propag.*, vol. 64, no. 2, pp. 543–553, Feb. 2016.

[23] D. Cavallo, W. H. Syed, and A. Neto, "Connected-slot array with artificial dielectrics: A 6 to 15 GHz dual-pol wide-scan prototype," *IEEE Trans. Antennas Propag.*, vol. 66, no. 6, pp. 3201–3206, Jun. 2018.

[24] S. M. Moghaddam, J. Yang, and A. U. Zaman, "Fully-planar ultrawideband tightly-coupled array (FPU-TCA) with integrated feed for wide-scanning millimeter-wave applications," *IEEE Trans. Antennas Propag.*, vol. 68, no. 9, pp. 6591–6601, Sep. 2020.

[25] M. H. Novak, F. A. Miranda, and J. L. Volakis, "Ultra-wideband phased array for millimeter-wave ISM and 5G bands, realized in PCB," *IEEE Trans. Antennas Propag.*, vol. 66, no. 12, pp. 6930–6938, Dec. 2018.
[26] Z. Jiang, S. Xiao, Z. Yao, and B.-Z. Wang, "A planar ultrawideband wide-angle scanning array loaded with polarization-sensitive frequency-selective surface structure," *IEEE Trans. Antennas Propag.*, vol. 68, no. 11, pp. 7348–7357, Nov. 2020.
[27] D.-M. Sun, Z.-C. Hao, C.-Y. Ding, R.-J. Liu, Z.-J. Guo, and H.-Y. Yin, "A low-profile ultra-wideband and wide-scanning phased array for UHF applications," *IEEE Trans. Antennas Propag.*, vol. 71, no. 1, pp. 473–486, Jan. 2023.
[28] A. O. Bah, P.-Y. Qin, R. W. Ziolkowski, Y. J. Guo, and T. S. Bird, "A wideband low-profile tightly coupled antenna array with a very high figure of merit," *IEEE Trans. Antennas Propag.*, vol. 67, no. 4, pp. 2332–2343, Apr. 2019.
[29] H. Zhang, S. Yang, S. Xiao, Y. Chen, and S. Qu, "Low-profile, lightweight, ultra-wideband tightly coupled dipole arrays loaded with split rings," *IEEE Trans. Antennas Propag.*, vol. 67, no. 6, pp. 4257–4262, Jun. 2019.
[30] J. Zhong, A. Johnson, E. A. Alwan, and J. L. Volakis, "Dual-linear polarized phased array with 9:1 bandwidth and 60° scanning off broadside," *IEEE Trans. Antennas Propag.*, vol. 67, no. 3, pp. 1996–2001, Mar. 2019.
[31] A. Ludwig, "The definition of cross polarization," *IEEE Trans. Antennas Propag.*, vol. AP-21, no. 1, pp. 116–119, Jan. 1973.
[32] J. A. Kasemodel, C.-C. Chen, and J. L. Volakis, "Wideband planar array with integrated feed and matching network for wide-angle scanning," *IEEE Trans. Antennas Propag.*, vol. 61, no. 9, pp. 4528–4537, Sep. 2013.
[33] S. B. Venkatakrishnan, E. A. Alwan, and J. L. Volakis, "Wideband RF self-interference cancellation circuit for phased array simultaneous transmit and receive systems," *IEEE Access*, vol. 6, pp. 3425–3432, 2018.
[34] D. M. Pozar, "Analysis of finite phased arrays of printed dipoles," *IEEE Trans. Antennas Propag.*, vol. AP-33, no. 10, pp. 1045–1053, Oct. 1985.
[35] H. Holter and H. Steyskal, "On the size requirement for finite phased-array models," *IEEE Trans. Antennas Propag.*, vol. 50, no. 6, pp. 836–840, Jun. 2002.
[36] M. N. Vouvakis and D. H. Schaubert, "Vivaldi antenna arrays," in *Frontiers in Antennas: Next Generation Design & Engineering*, F. B. Gross, Ed. New York, NY, USA: McGraw-Hill, 2011.
[37] E. Holzman, "On the use of dummy elements to match edge elements in transmit arrays," in *Proc. IEEE Int. Symp. Phased Array Syst. Technol.*, Oct. 2013, pp. 549–552.
[38] Q. Chen, Z. Li, W. Wang, Z. Huang, X. Liang, and X. Wu, "A broadband dual-polarized solar cell phased array antenna," *IEEE Trans. Antennas Propag.*, vol. 70, no. 1, pp. 353–364, Jan. 2022.
[39] R. C. Hansen, *Phased Array Antennas*. Hoboken, NJ, USA: Wiley, 2009, ch. 15, pp. 526–527.
[40] L. Li, J.-B. Yan, C. O'Neill, C. D. Simpson, and S. P. Gogineni, "Coplanar side-fed tightly coupled ultra-wideband array for polar ice sounding," *IEEE Trans. Antennas Propag.*, vol. 70, no. 6, pp. 4331–4341, Jun. 2022.

De-Ming Sun (Graduate Student Member, IEEE) received the B.S. degree from the School of Information and Communication Engineering, North University of China, Taiyuan, China, in 2015, and the M.S. degree in electromagnetic field and microwave technology from the University of Electronic Science and Technology of China, Chengdu, China, in 2018. He is currently pursuing the Ph.D. degree in electromagnetic field and microwave technology with Southeast University, Nanjing, China.

His current research interests include microwave and millimeter-wave passive components and antennas, ultrawideband phased arrays, RF circuit design, multibeam antennas, and antenna array decoupling techniques.

Zhang-Cheng Hao (Senior Member, IEEE) received the B.S. degree in microwave engineering from Xidian University, Xi'an, China, in 1997, and the M.S. and Ph.D. degrees in radio engineering from Southeast University, Nanjing, China, in 2002 and 2006, respectively.

In 2006, he was a Post-Doctoral Researcher with the Laboratory of Electronics and Systems for Telecommunications (LEST), École Nationale Supérieure des Télécommunications de Bretagne (ENSTB), Bretagne, France, where he was involved with developing millimeter-wave antennas. In 2007, he joined the Department of Electrical, Electronic and Computer Engineering, Heriot-Watt University, Edinburgh, U.K., as a Research Associate, where he was involved with developing multilayer integrated circuits and ultrawideband components. In 2011, he joined the School of Information Science and Engineering, Southeast University, as a Professor. He holds 20 granted patents and has authored and coauthored over 200 referred journals and conference papers. His current research interests involve microwave and millimeter-wave systems, massive multiple-beam array antennas, submillimeter-wave and terahertz components, and passive circuits.

Dr. Hao is a member of the IEEE MTT-21 Terahertz Technology and Applications, Technical Committees. He has served as the TPC Chair/ Co-Chair for many international conferences, such as the iWat2018, the ICMMT 2019, and the ISAP 2019. He has served as a Reviewer for many technique journals, including the IEEE TRANSACTIONS ON MICROWAVE THEORY AND TECHNIQUES (T-MTT), IEEE TRANSACTIONS ON ANTENNAS AND PROPAGATION (T-AP), IEEE ANTENNAS AND WIRELESS PROPAGATION LETTERS (AWPL), and IEEE MICROWAVE AND WIRELESS COMPONENTS LETTERS (MWCL), a Guest Editor for the IEEE T-MTT special issue on IWS 2018, and an Associate Editor for the *IET Electronics Letters* and the *IET Microwaves, Antennas, & Propagation*.

Wen-Ye Liu (Graduate Student Member, IEEE) received the B.S. degree from the School of Electronic Engineering, Xidian University, Xi'an, China, in 2020. He is currently pursuing the Ph.D. degree with the State Key Laboratory of Millimeter Waves, Southeast University, Nanjing, China.

His current research interests include microwave and millimeter-wave radar systems, microwave and millimeter-wave antennas, phased arrays, and ultrawide-angle scanning technology.

Chen-Yu Ding (Graduate Student Member, IEEE) was born in Shandong, China, in 1998. He received the B.S. degree in electromagnetic fields and wireless technology from Northwestern Polytechnical University, Xi'an, China, in 2020. He is currently pursuing the Ph.D. degree with the State Key Laboratory of Millimeter Waves, Southeast University, Nanjing, China.

His current research interests include antenna arrays, multibeam antennas, and terahertz technology.